Wounded cells drive rapid epidermal repair in the early *Drosophila* embryo

Rodrigo Fernandez-Gonzalez[a,b] and Jennifer A. Zallen[c]
[a]Institute of Biomaterials and Biomedical Engineering and Department of Cell and Systems Biology, University of Toronto, Toronto, ON M5S 3G9, Canada; [b]Developmental and Stem Cell Biology Program, The Hospital for Sick Children, Toronto, ON M5G 1X8, Canada; [c]Howard Hughes Medical Institute, Developmental Biology Program, Sloan-Kettering Institute, New York, NY 10065

ABSTRACT **Epithelial tissues are protective barriers that display a remarkable ability to repair wounds. Wound repair is often associated with an accumulation of actin and nonmuscle myosin II around the wound, forming a purse string. The role of actomyosin networks in generating mechanical force during wound repair is not well understood. Here we investigate the mechanisms of force generation during wound repair in the epidermis of early and late *Drosophila* embryos. We find that wound closure is faster in early embryos, where, in addition to a purse string around the wound, actomyosin networks at the medial cortex of the wounded cells contribute to rapid wound repair. Laser ablation demonstrates that both medial and purse-string actomyosin networks generate contractile force. Quantitative analysis of protein localization dynamics during wound closure indicates that the rapid contraction of medial actomyosin structures during wound repair in early embryos involves disassembly of the actomyosin network. By contrast, actomyosin purse strings in late embryos contract more slowly in a mechanism that involves network condensation. We propose that the combined action of two force-generating structures—a medial actomyosin network and an actomyosin purse string—contributes to the increased efficiency of wound repair in the early embryo.**

Monitoring Editor
Richard Fehon
University of Chicago

Received: May 2, 2013
Revised: Aug 5, 2013
Accepted: Aug 19, 2013

INTRODUCTION

Epithelial tissues serve as protective barriers that respond rapidly to wounds. It has long been recognized that wound repair is often faster in embryos than in adults (Longaker *et al.*, 1990; Whitby and Ferguson, 1991; McCluskey and Martin, 1995). The basis for this difference is not well understood. Epithelial repair of multicellular wounds in fly, frog, chick, and mouse embryos is accompanied by an accumulation of actin and myosin II around the wound, forming a multicellular cable that has been proposed to act as a purse string that draws the wound closed (Martin and Lewis, 1992; McCluskey and Martin, 1995; Kiehart *et al.*, 2000; Davidson *et al.*, 2002; Wood *et al.*, 2002). Actomyosin purse strings are also present during wound closure by cells in culture (Bement *et al.*, 1993) and in adult epithelia such as the cornea (Danjo and Gipson, 1998) and gut (Russo *et al.*, 2005), where they are important for the repair of incisional wounds and ulcers. The actomyosin purse strings that form around multicellular wounds in the *Xenopus* embryo, however, do not generate mechanical force (Davidson *et al.*, 2002), raising the question of whether they contribute functionally to wound repair. The cell behaviors required to generate the mechanical forces that drive epithelial wound repair remain unclear.

Force-generating actomyosin networks display a range of architectures and contract through distinct mechanisms. For example, apical constriction can be driven by an actomyosin band around the apical circumference of the cell (Burnside, 1971; Hildebrand, 2005) or a medial meshwork of actin and myosin filaments that span the apical cell surface (Martin *et al.*, 2009). Actomyosin networks in some cases actively disassemble their component actin and myosin filaments as they contract (network disassembly). Other networks contract by concentrating a constant number of actin and myosin filaments into a smaller volume (network condensation). Contraction

This article was published online ahead of print in MBoC in Press (http://www.molbiolcell.org/cgi/doi/10.1091/mbc.E13-05-0228) on August 28, 2013.

Address correspondence to: Rodrigo Fernandez-Gonzalez (rodrigo.fernandez.gonzalez@utoronto.ca), Jennifer A. Zallen (zallenj@mskcc.org).

Abbreviations used: GFP, green fluorescent protein; SIESTA, Scientific Image Segmentation and Analysis.

© 2013 Fernandez-Gonzalez and Zallen. This article is distributed by The American Society for Cell Biology under license from the author(s). Two months after publication it is available to the public under an Attribution–Noncommercial–Share Alike 3.0 Unported Creative Commons License (http://creativecommons.org/licenses/by-nc-sa/3.0).

"ASCB®," "The American Society for Cell Biology®," and "Molecular Biology of the Cell®" are registered trademarks of The American Society of Cell Biology.

of the cytokinetic ring during early cell divisions in *Caenorhabditis elegans* (Carvalho *et al.*, 2009), medial actomyosin networks in intercalating cells (Fernandez-Gonzalez and Zallen, 2011), and mesoderm precursors in *Drosophila* (Mason *et al.*, 2013) is associated with network disassembly. By contrast, cytokinetic rings in *Dictyostelium* (Robinson *et al.*, 2002; Reichl *et al.*, 2008), *Schizosaccharomyces pombe* (Wu *et al.*, 2003), and *Neurospora crassa* (Calvert *et al.*, 2011) contract through network condensation. Different mechanisms of contraction may be associated with differences in the magnitude, dynamics, or regulation of the mechanical forces generated during contraction. It is unknown which mechanisms of actomyosin contraction operate during wound repair.

In this study we investigate epidermal wound repair in the *Drosophila* embryo and find that multicellular wounds heal faster at early stages of embryonic development. Wound repair in early embryos is associated with actomyosin networks at the medial cortex of the wounded cells, whose contraction drives rapid wound closure in parallel with a loss of actomyosin filaments. By contrast, wound repair in late embryos is driven by the assembly of an actomyosin purse string at the wound margin, which contracts more slowly in a mechanism that involves actomyosin condensation. Both structures generate mechanical force, and medial actomyosin networks in early embryos generate greater contractile force than purse strings. We propose that the combined action of these two actomyosin networks contributes to the increased efficiency of wound repair in early embryos.

RESULTS

Quantitative imaging reveals rapid wound closure in early *Drosophila* embryos

To investigate how wounds heal in developing epithelial tissues undergoing active morphogenetic movements, we compared multicellular wound closure and cytoskeletal dynamics in the epidermis of early *Drosophila* embryos during axis elongation (stages 7–8) with *Drosophila* embryos at later stages of epithelial maturation (stages 14–15). We wounded the epidermis using an ultraviolet laser to generate a 7- to 8-µm linear lesion across a single cell interface (Figure 1, A and B). We analyzed the dynamics of wound closure using the LiveWire image segmentation algorithm (Fernandez-Gonzalez and Zallen, 2011) to rapidly delineate wound margins in time-lapse movies (Figure 1C).

To compare the rates of wound closure in early and late embryos, we measured the time necessary for wound area to reach 50 μm^2 (15–25% of the maximum wound size). We found that wound closure was faster on average in early embryos (Figure 1D). Wound area reached 50 μm^2 in 11.6 ± 2.1 min (mean ± SEM) in early embryos, less than half the time necessary to reach this size in late embryos (25.9 ± 3.1 min, $p = 0.0015$). There was no significant difference in maximum wound size in early (266 ± 41 μm^2) and late (320 ± 42 μm^2) embryos, and wounds with a similar maximum size closed faster in early embryos (Figure 1, E and F), demonstrating that faster wound closure in early embryos is not due to differences in wound size. Wound repair occurred in two phases: an initial fast phase and a subsequent slow phase (Figure 1G). Although both phases were observed in early and late embryos, the fast phase was shorter (Figure 1H) and faster (Figure 1I) in the early embryo, resulting in a more dramatic transition between phases. In early embryos, wounds initially contracted at a rate of 37.8 ± 5.0 μm^2/min in the fast phase and a significantly slower rate of 3.1 ± 0.8 μm^2/min in the slow phase ($p = 8 \times 10^{-5}$). The fast phase was significantly slower in late embryos (15.7 ± 3.2 μm^2/min, $p = 0.002$), but the rate of contraction during the slow phase was similar to that in early embryos (3.3 ± 0.8 μm^2/min in late embryos). These results demonstrate that the rate of wound repair decreases as *Drosophila* embryos develop.

Wounded cells in early embryos assemble medial actomyosin networks

To maintain epithelial continuity, wounded cells must be extruded from the epidermis. Cells can leave an epithelium via extrusion from the apical or the basal surface of the tissue. The direction of extrusion is determined by the position of the contractile machinery (Slattum *et al.*, 2009). To determine how wounded cells exit the epidermis during wound repair in *Drosophila*, we imaged wound closure in three dimensions (Supplemental Figure S1). Wounded cells in early embryos constricted at their apical surface, rounded up, and shifted their volume basally (Supplemental Figure S1, 7.5 min), disappearing from the apical surface of the epithelium and moving basally at a speed of ~0.5 µm/min (Supplemental Figure S1, 15 min). Extruding cells were not detected after wounding in late embryos, possibly due to the rapid phagocytosis of wounded cells by hemocytes (Supplemental Figure S2; Stramer *et al.*, 2005; Wood *et al.*, 2006; Moreira *et al.*, 2010). Wounded cells in the early embryo are therefore extruded basally through apical constriction.

The forces that drive the apical constriction of wounded cells in the early embryo could be provided by the wounded cells themselves or by the surrounding tissue. To distinguish between these possibilities, we investigated myosin localization and dynamics during wound repair in embryos expressing myosin:mCherry and the green fluorescent protein (GFP) fused to E-cadherin. In early and late embryos, cells adjacent to the wound assembled a myosin purse string around the wound (Figure 2, A and B). The myosin purse string formed faster in early embryos, reaching 50% of its maximum intensity at 299 ± 58 s after wounding, compared with 577 ± 77 s in late embryos ($p = 0.012$, $n = 10$–13 wounds). The myosin purse string appeared more fragmented in early embryos, failing to form a smooth, continuous boundary around the wound (Figure 2A). Of note, myosin also accumulated at the medial surface of wounded cells during the fast phase of wound closure in early embryos (Figure 2A and Supplemental Movie S1). Medial myosin puncta converged from the periphery of the wounded cell toward the center (Figure 2A and Supplemental Movie S1), suggesting that this pool of protein does not contribute to the purse string. Medial myosin was not observed inside wounds in late embryos (Figure 2B and Supplemental Movie S2). These results suggest that two populations of myosin—a myosin purse string around the wound and medial myosin networks in the wounded cells—contribute to wound closure in early embryos.

To explore the role of cells around the wound in wound closure, we used watershed image segmentation (Fernandez-Gonzalez and Zallen, 2011) to quantify apical area changes in cells adjacent to the wound border (adjacent cells) and cells one to five cell diameters away (distant cells). Immediately after wounding, the apical area of adjacent cells increased by 7.3 ± 4% and the apical area of distant cells decreased by 3.5 ± 1%, resulting in a net decrease in the area of the epithelium surrounding the wound ($p = 0.01$; Supplemental Figure S3A). The apical areas of adjacent cells decreased by 20.5 ± 6% of their initial value within 3 min of wounding, and the apical areas of distant cells decreased by 9.6 ± 2% within 5 min of wounding (Supplemental Figure S3A). Of note, wound closure did not start until the apical areas of both adjacent and distant cells had stabilized, indicating that changes in the apical area of cells around the wound do not contribute directly to wound repair (Supplemental Figure S3B).

The absence of medial contractile networks in wounded cells in late embryos could be caused by differences in the severity of the

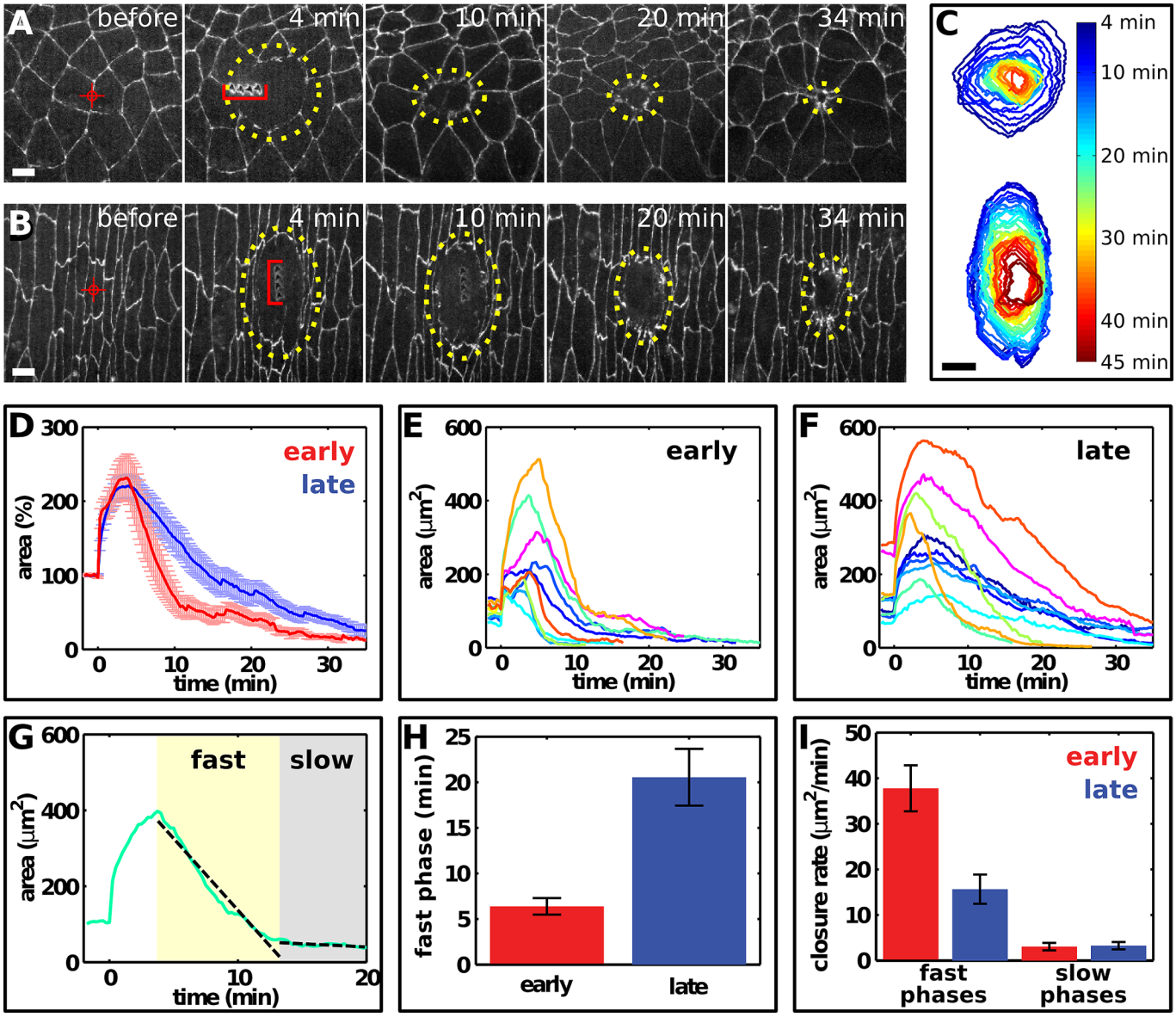

FIGURE 1: Wound closure is faster in early *Drosophila* embryos. (A, B) Epidermal cells expressing E-cadherin:GFP in a stage 7 (A, early) and a stage 14 (B, late) embryo. Red targets indicate the interface ablated for wounding. Yellow dots delineate the wound. The time after wounding is indicated. Red brackets at $t = 4$ min indicate laser-induced holes in the vitelline membrane. Wounded cells move away from the wound site (A) due to cell rearrangement. Anterior, left; dorsal, up. Bars, 5 μm. (C) Wound healing in early (top) and late (bottom) embryos, corresponding to image sequences in A and B, respectively. Wound perimeter was measured at 1-min intervals using the LiveWire algorithm. Bar, 5 μm. (D) Wound area normalized to the total area of the prewounded cells in early ($n = 9$, red) and late ($n = 10$, blue) embryos. Error bars, SEM. (E, F) Wound area over time in early (E) and late (F) embryos. Different colors indicate different wounds. $t = 0$ min is the time of wounding. (G) Linear fits (black, dashed lines) to the fast and slow phases of wound closure (green). The rates of wound closure during the fast (yellow shade) and slow (gray shade) phases were calculated as the slopes of these lines. (H) Duration of the fast phase in early ($n = 9$, red) and late ($n = 10$, blue) embryos. Error bars, SEM. (I) Wound closure rate in the fast (left) and slow (right) phases of wound closure in early ($n = 9$, red) and late ($n = 10$, blue) embryos. Error bars, SEM.

wound or a lack of medial myosin before wounding. In late embryos, laser-induced wounds damage a larger fraction of the cell surface, as cells at this stage have a smaller apical area (Supplemental Figure S4, A–C). To address the possibility that medial myosin networks do not form in late embryos due to increased laser damage, we wounded late embryos using the minimum laser power that elicited a response (Supplemental Movie S3). Reduced-intensity wounds in late embryos still resulted in the assembly of a myosin purse string, but medial networks were not observed in the wounded cells, suggesting that the absence of a medial network is not due to increased damage to these cells. Wound healing in early embryos could also involve a distinct, single-cell wound response (Bement *et al.*, 1999; Abreu-Blanco *et al.*, 2011). To test this possibility, we induced wounds within single cells in late embryos, preserving the cell boundaries. Single-cell wounds resulted in the assembly of a myosin purse string around the wounded cell, but medial networks did not

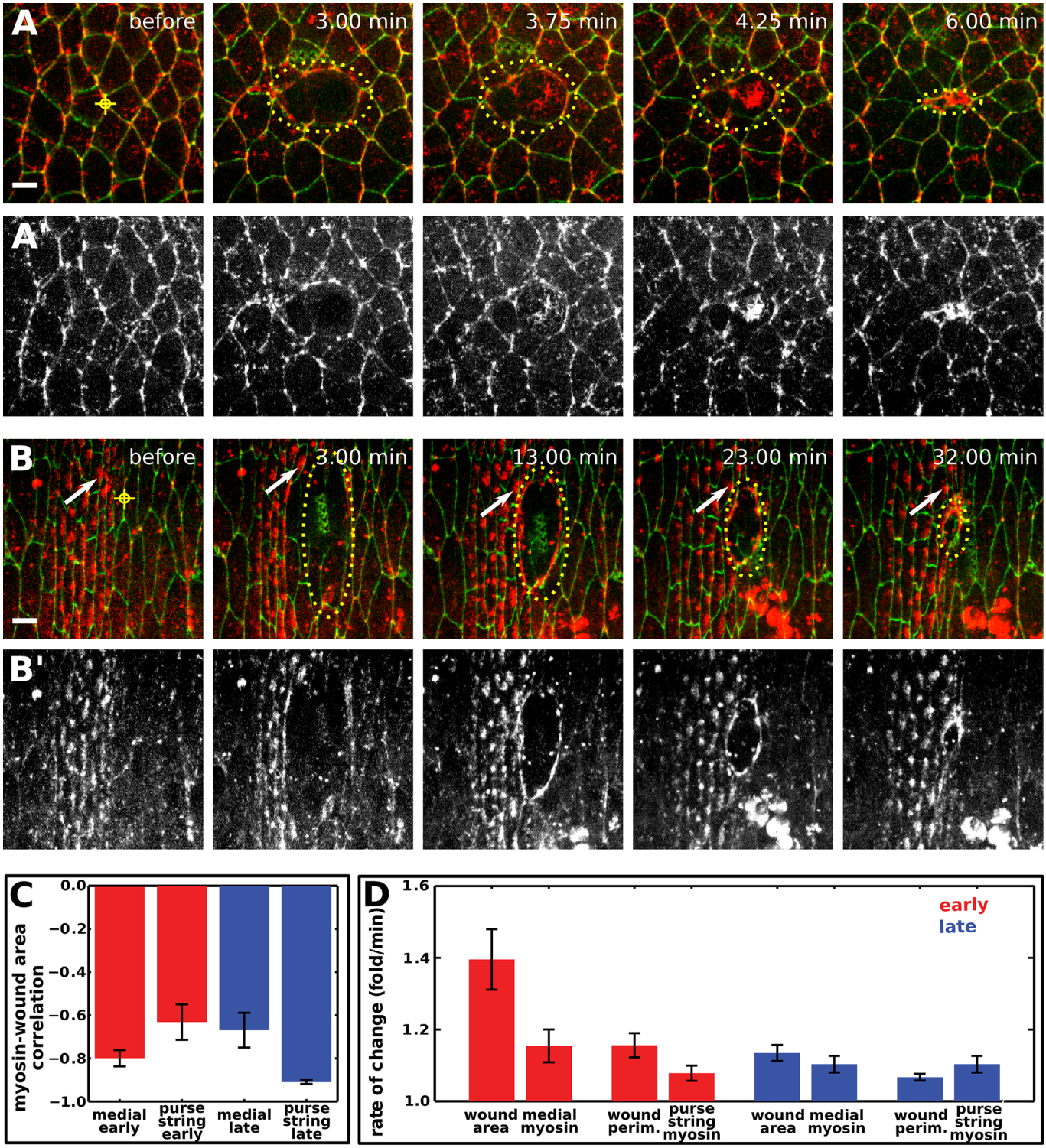

FIGURE 2: Distinct myosin structures form during epidermal wound closure in early and late *Drosophila* embryos. (A, B) Epidermal cells expressing E-cadherin:GFP and myosin:mCherry in a stage 7 (A) and a stage 14 (B) embryo. The time after wounding is indicated. Yellow target indicates the site of wounding, dots delineate the wound margin. White arrows track the position of a denticle precursor. Anterior, left; dorsal, up. Bars, 5 μm. (A′, B′) The myosin:mCherry signal in A and B. (C) Correlation coefficient between wound area and mean myosin fluorescence in the wounded cells or the purse string in early ($n = 10$, red bars) and late ($n = 8$, blue bars) embryos. Error bars, SEM. (D) Rate of change of wound area, perimeter, or mean myosin fluorescence in the medial region of wounded cells or at the purse string in early ($n = 10$, red bars) and late ($n = 8$, blue bars) embryos. The rate of wound area contraction is the average ratio of area(t – 1 min)/area(t). Perimeter reduction was similarly quantified. The rate of increase in mean myosin fluorescence was quantified with the ratio myosin(t)/myosin(t – 1 min) to account for the fact that area and mean fluorescence are inversely correlated. Error bars, SEM.

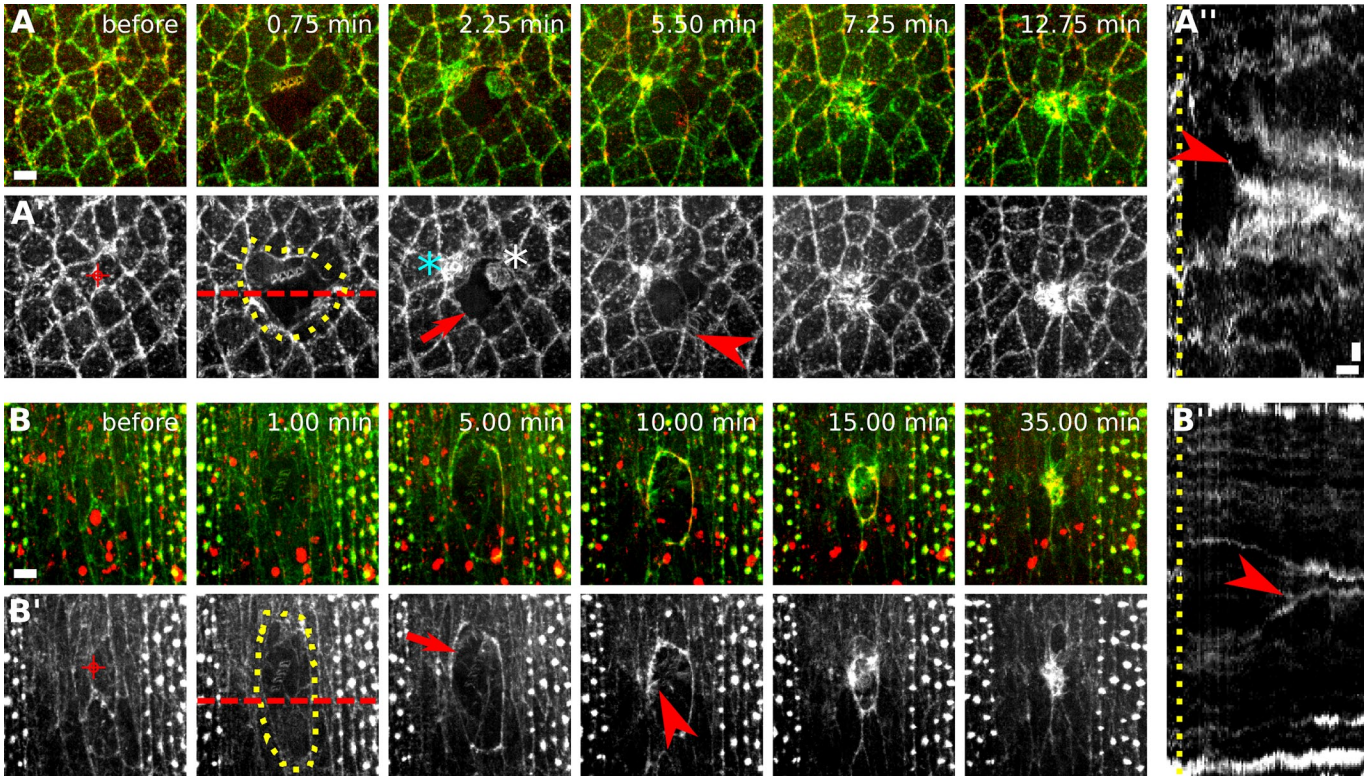

FIGURE 3: Complex actin dynamics during embryonic wound closure in *Drosophila*. (A, B) Epidermal cells expressing GFP:moesin (green) to visualize filamentous actin and myosin:mCherry (red) in a stage 7 (A) and a stage 14 (B) embryo. The time after wounding is indicated. Anterior, left; dorsal, up. Bars, 5 μm. (A′, B′) GFP:moesin signal in A and B. Red targets indicate the interface ablated for wounding. Yellow dots delineate the wound outline. Actin accumulates around the wound (arrows), at the medial cortex of wounded and adjacent cells (cyan and white asterisk, respectively), and in protrusions (arrowheads). (A″, B″) Kymographs showing the pattern of GFP:moesin along the red dashed lines in A′ and B′. Yellow line indicates time of wounding. Arrowheads indicate protrusions formed by wounded cells (A″) or cells adjacent to the wound (B″). Anterior, down. Bars, horizontal, 3 min; vertical, 2 μm.

form (Supplemental Movie S4). Finally, we confirmed that medial myosin is present in the late embryonic epidermis (Supplemental Figure S4, D–F), indicating that these cells are competent to assemble medial networks. Therefore differences in the damage caused by the wound or the lack of medial myosin do not explain the absence of contractile networks in wounded cells in late embryos.

Actomyosin contractility is necessary for rapid wound repair in early embryos

Our results demonstrate that two distinct myosin networks are present during wound healing in early embryos. To address whether either of these structures contributes to wound closure, we first analyzed myosin dynamics in the medial and purse-string networks. In early and late embryos, mean myosin fluorescence in medial and purse-string structures increased as wound area and perimeter decreased (Figure 2C). In late embryos, the anticorrelation between wound area and purse-string myosin fluorescence was significantly stronger than the anticorrelation between wound area and residual myosin at the medial cortex (–0.91 ± 0.01 vs. –0.67 ± 0.08, respectively, $p = 0.017$; Figure 2C). Wound healing in early embryos showed the opposite trend: the anticorrelation between wound area and medial myosin fluorescence was significantly stronger than the anticorrelation between wound area and purse–string myosin (–0.80 ± 0.04 vs. –0.63 ± 0.08, respectively, $p = 0.019$; Figure 2C). These results show that wound closure in early embryos is more strongly correlated with medial myosin levels, whereas wound closure in late embryos is more strongly correlated with myosin levels in the purse string.

Actin structures also displayed different dynamics in early and late embryos. We investigated the dynamics of filamentous actin (F-actin) during wound closure using a GFP fusion to the F-actin–binding domain of moesin (Kiehart *et al.*, 2000). Like myosin, F-actin accumulated at the wound margin in early and late embryos (Figure 3, A and B, arrows) and at the apical surface of wounded cells and some cells adjacent to the wound in early embryos (Figure 3A″). In late embryos, cells around the wound assembled filopodia that extended into the wound (Figure 3, B–B″, arrowheads; Wood *et al.*, 2002; Abreu-Blanco *et al.*, 2012; Pickering *et al.*, 2013). In early embryos, wounded cells appeared to assemble actin protrusions pointing outward from the wound (Figure 3, A–A″, arrowheads) and blebs (Supplemental Movie S5). These experiments reveal complex actin dynamics during wound repair and provide further evidence that wounded cells in the early embryo may actively participate in wound closure.

The observation that dynamic actomyosin networks form during wound healing raises the question of whether actomyosin contractility could drive wound repair. In late *Drosophila* embryos, contractile actomyosin networks accelerate wound repair but are not essential for wounds to close (Wood *et al.*, 2002; Abreu-Blanco *et al.*, 2012). Furthermore, myosin could contribute to wound healing through alternative mechanisms, such as the regulation of actin organization and cross-linking (Burkel *et al.*, 2012; Ma *et al.*, 2012) or actin-based protrusions (Wood *et al.*, 2002; Abreu-Blanco *et al.*, 2012).

Rho-kinase activates myosin directly by phosphorylating the myosin light chain (Amano *et al.*, 1996) and indirectly by inhibiting the myosin phosphatase (Kimura *et al.*, 1996). To determine whether myosin contractile activity is necessary for rapid wound repair in early *Drosophila* embryos, we injected the Rho-kinase inhibitor Y-27632 into early embryos 1–3 min after wounding to specifically inhibit myosin activity during wound closure. In contrast with water-injected embryos, inhibition of Rho-kinase led to an immediate loss of junctional and medial myosin in epidermal cells (Figure 4, A and B) and a cessation of wound closure (Figure 4C). Small changes in wound area were observed due to relaxation of the cells around the wound (Figure 4B). These results demonstrate that contraction of actomyosin networks is necessary for wound repair in the early embryo and provide further evidence that the mechanisms of wound repair change as embryos develop.

Wounded cells exert contractile forces that promote wound repair in early embryos

The dynamic myosin and actin networks in wounded cells are consistent with a model in which medial and purse-string networks actively participate in wound closure in early embryos. Not all actomyosin structures during wound closure, however, are contractile (Davidson *et al.*, 2002). To determine which myosin networks are functionally important for wound closure, we used laser ablation to investigate whether myosin structures generate force during wound healing. We previously showed that cells in the early embryo display uniform viscoelastic properties (Fernandez-Gonzalez *et al.*, 2009). Under these conditions, the initial recoil velocity after laser ablation is proportional to the tension acting on the network (Hutson *et al.*, 2003). To estimate the tension acting on medial myosin networks in wounded cells in early embryos, we ablated these networks ~2 min after the onset of medial myosin accumulation (Figure 5A). Using particle image velocimetry (Raffel *et al.*, 2007), we observed radial recoil velocities of 160 ± 13 nm/s (Figure 5, A, C, and E). When medial myosin networks were ablated, wounds stopped healing and expanded at an initial rate of 6.1 ± 0.7 $\mu m^2/s$ (Figure 5D). These results demonstrate that the medial myosin networks in wounded cells exert forces on the wound margin and that these forces actively contribute to tissue repair.

To evaluate the contributions of different myosin structures to wound closure, we compared the recoil velocities after ablation of the medial surface of wounded cells or the purse strings around wounds. In early embryos, ablation of medial myosin networks in wounded cells resulted in recoil velocities that were 1.5 times greater than the recoil velocities after ablation of the purse string ($p = 0.009$; Figure 5, A and E), indicating that wounded cells generate greater local forces. By contrast, ablation of purse strings in late embryos resulted in recoil velocities that were 1.8 times greater than the recoil velocities at the medial surface of the wounded cells ($p = 0.070$; Figure 5, B and E), consistent with the absence of detectable myosin in wounded cells. Together these results demonstrate that contractile medial actomyosin networks in wounded cells contribute to rapid wound healing in early embryos, and this contribution is greater than that of the purse string around the wound.

Rapid contraction is associated with disassembly of actomyosin networks

Our data demonstrate that actomyosin contractility drives rapid wound repair in the early *Drosophila* embryo. But the mechanisms of actomyosin network contraction during wound repair are unclear. To investigate how actomyosin networks contract during wound repair, we quantified changes in myosin and F-actin fluorescence during wound closure in embryos expressing myosin:mCherry and GFP:moesin. In early embryos, the total myosin and F-actin fluorescence in wounded cells decreased rapidly during closure, in parallel

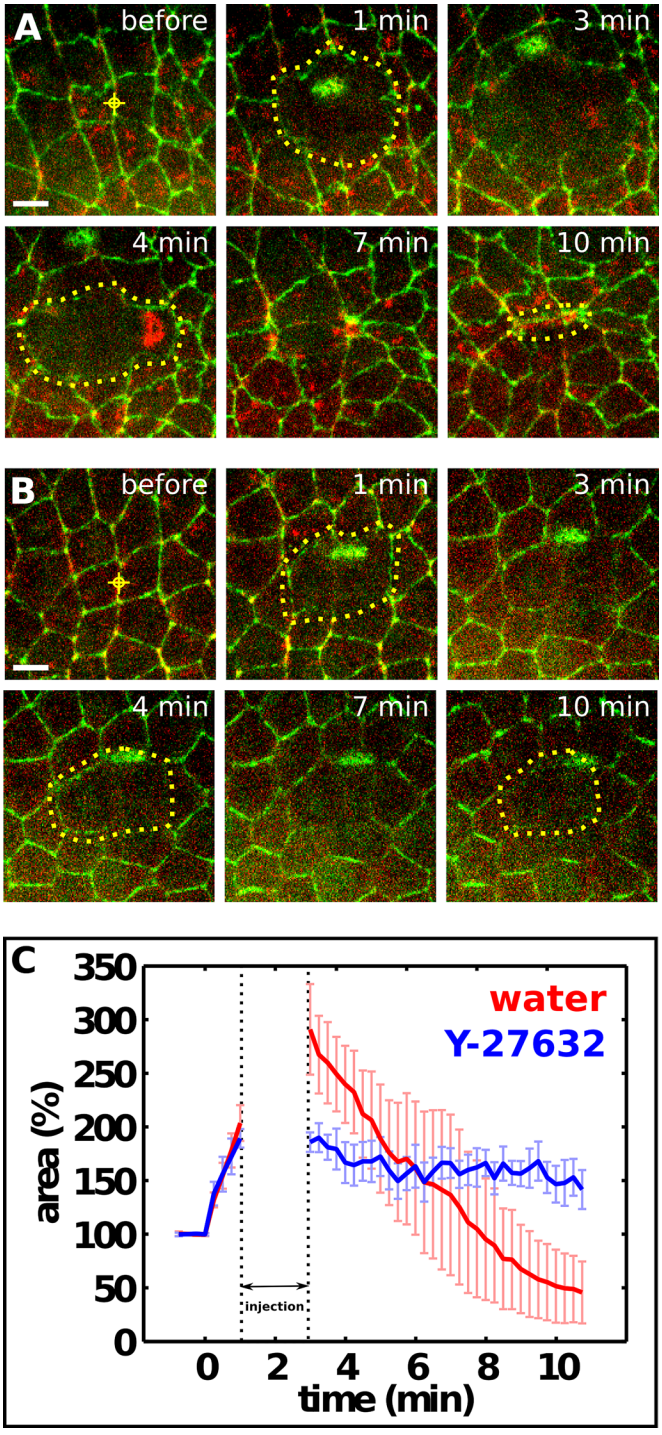

FIGURE 4: Myosin activity is necessary for rapid wound repair in early embryos. (A, B) Epidermal cells expressing E-cadherin:GFP and myosin:mCherry in stage 7 embryos injected with water (A) or 100 mM of the Rho-kinase inhibitor Y-27632 (B). Red targets indicate the interface ablated for wounding. Yellow dots delineate the wound in alternating time points. The time after wounding is indicated. Injection is between 1 and 3 min. Anterior, left; dorsal, up. Bars, 5 μm. (C) Wound area normalized to the total area of the prewounded cells in embryos injected with water ($n = 5$, red) or 100 mM Y-27632 ($n = 4$, blue). The dotted lines delimit the time of injection. Error bars, SEM.

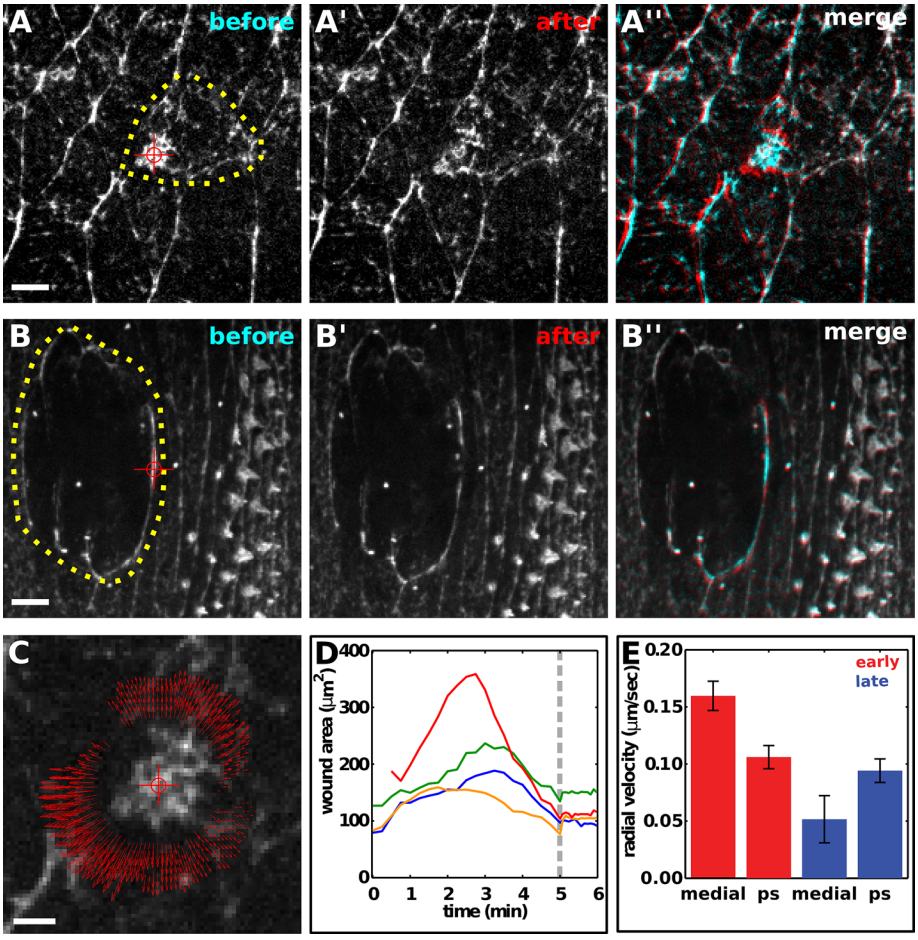

FIGURE 5: Contractile actomyosin networks in wounded cells drive epidermal repair in early *Drosophila* embryos. (A–A″, B–B″) Epidermal cells expressing myosin:GFP in a wounded stage 7 (A) or stage 14 (B) embryo. Yellow dots delineate the wound margin, red targets indicate the site of ablation. Myosin networks are shown immediately before ablation (A, B) and 3.3 s after ablation (A′, B′). (A″, B″) Overlay of images before (cyan) and after (red) ablation of myosin networks. Anterior, left; dorsal, up. Bars, 5 μm. (C) Particle image velocimetry analysis of the response to ablation in A. Red target indicates the site of ablation, red arrows indicate the direction and magnitude of recoil. Bar, 2 μm. (D) Wound area over time in early embryos. Medial actomyosin networks that form after wounding were ablated at the time indicated by the gray line. (E) Radial recoil velocity after spot ablation of distinct myosin networks during wound repair. Red bars correspond to medial networks in wounded cells (medial, $n = 8$) and purse strings around wounds in early embryos (ps, $n = 6$); blue bars correspond to the medial surface of the wounded cells (medial, $n = 6$) and purse strings around wounds in late embryos (ps, $n = 8$). Error bars, SEM.

with the reduction in wound area (Figure 6, A, D, and E). By contrast, in late embryos, myosin and F-actin fluorescence in the purse string remained relatively constant or decreased slowly during closure (Figure 6, B, H and I). The fold change in total myosin fluorescence during medial network contraction in early embryos was 24.4 ± 10.4, significantly greater than the fold change in total myosin fluorescence during purse-string contraction in late embryos, which was 2.6 ± 0.04 (Figure 6L; $p = 0.01$). Similar results were obtained for F-actin, which decreased 14.3 ± 4.4 fold in medial networks in early embryos and 2.3 ± 0.4 fold in purse strings in late embryos (Figure 6L; $p = 0.01$). Medial networks decreased in area and became dimmer as they contracted (Figure 6M), whereas purse strings became thicker and brighter (Figure 6N). Together these results suggest that medial and purse-string networks during wound healing contract through different mechanisms.

Actomyosin networks that contract by condensation should display mean myosin fluorescence that increases at a similar rate to the rate of wound closure. By contrast, actomyosin networks that contract by disassembly should have a mean myosin intensity that does not change or increases slowly compared with the rate of wound closure. In early embryos, mean myosin fluorescence in wounded cells increased at a rate of 1.15 ± 0.05 fold/min during closure, slower than the decrease in wound area (1.40 ± 0.08 fold/min, $p = 0.009$; Figures 2D and 6, A and F). Mean myosin fluorescence in the purse string in early embryos also increased more slowly than the decrease in wound perimeter (1.08 ± 0.02 vs. 1.16 ± 0.03 fold/min, respectively, $p = 0.006$; Figure 2D). These data suggest that medial and purse-string actomyosin networks are disassembled during contraction. These differences were observed for both myosin and F-actin throughout wound closure in early embryos (Figure 6, F and G, insets). By contrast, in late embryos mean myosin fluorescence in wounded cells increased at a rate of 1.10 ± 0.02 fold/min, similar to the rate of change of wound area (1.14 ± 0.02 fold/min, $p = 0.16$; Figure 2D), and mean myosin fluorescence in the purse string increased at 1.10 ± 0.02 fold/min, similar to the rate at which wound perimeter decreased (1.07 ± 0.01 fold/min, $p = 0.10$; Figures 2D and 6, B and J). Wound perimeter and myosin and F-actin fluorescence at the purse string changed at a similar rate during most of wound closure (Figure 6, J and K, insets). These results suggest that medial actomyosin networks in wounded cells in early embryos contract through disassembly, whereas purse-string contraction in late embryos occurs primarily through condensation (Figure 6C). These data indicate that embryonic development brings about changes in the mechanisms of actomyosin network contraction during wound repair.

DISCUSSION

Here we provide evidence that the closure of multicellular wounds in the *Drosophila* embryo is significantly faster at early stages of development and is associated with distinct cellular structures and actomyosin network properties. In late embryos, cells adjacent to the wound form an actomyosin purse string that contracts by network condensation. By contrast, early embryos form a purse string around the wound and medial actomyosin networks in the wounded cells that contract by network disassembly. Laser ablation experiments demonstrate that medial networks and purse strings both generate force. By comparing the magnitude of the forces generated by these structures, we demonstrate that medial actomyosin networks in wounded cells make the dominant contribution to wound closure in early embryos, indicating that wounded cells can actively drive wound repair. This is in contrast with the late embryo,

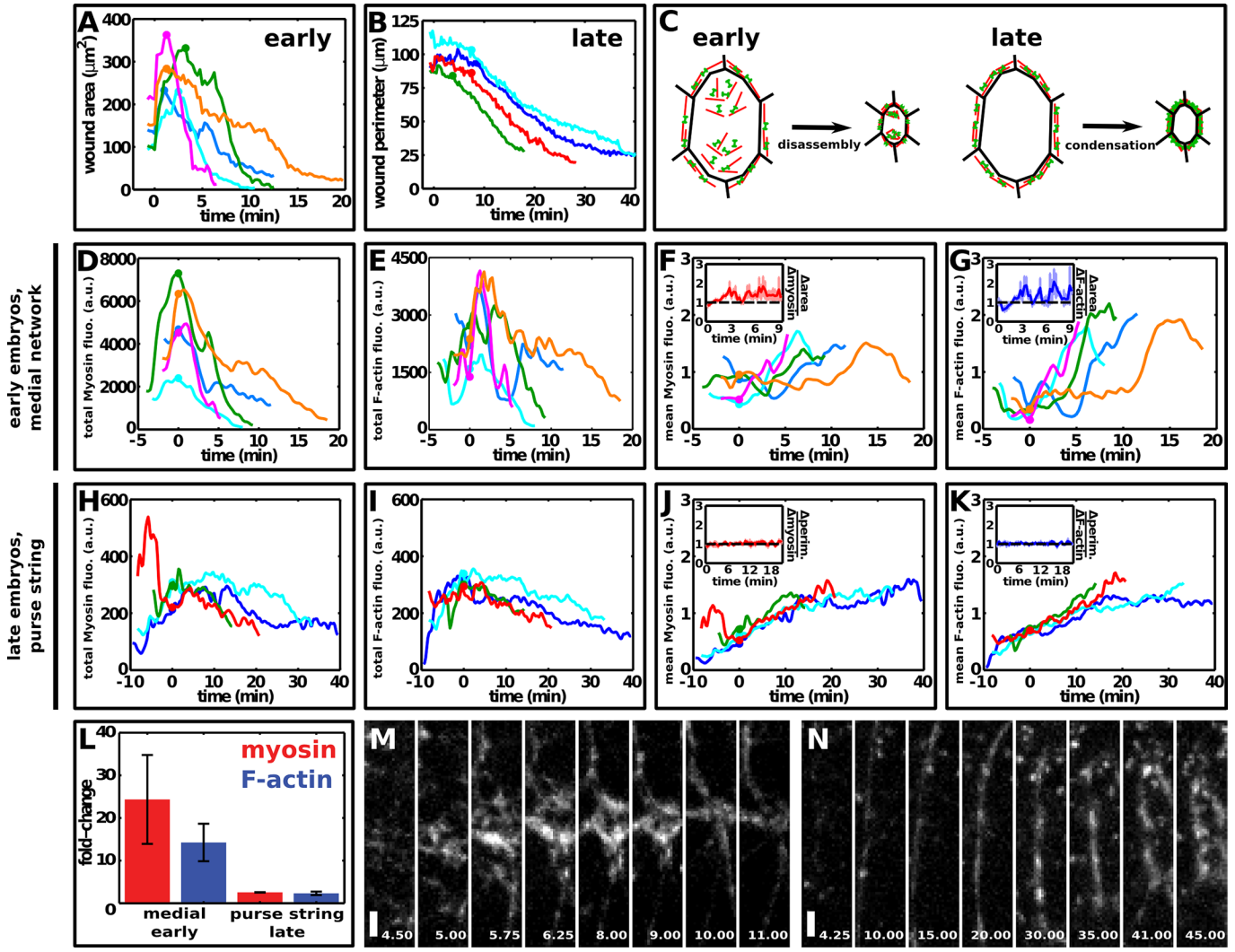

FIGURE 6: Distinct F-actin and myosin dynamics during embryonic wound closure in early and late embryos. (A, B) Wound area over time in early embryos (A) and wound perimeter over time in late embryos (B). $t = 0$ min is the time of wounding. (C) Model of wound closure in early and late embryos. (D, E) Total myosin (D) and F-actin (E) fluorescence in the medial cortex of wounded cells in early embryos decreased rapidly during wound closure. (F, G) Mean myosin (F) and F-actin (G) fluorescence in the medial cortex of wounded cells in early embryos increased during wound closure. Insets, ratio of the rates of change of wound area to the rate of change of mean myosin (F) or F-actin (G) fluorescence. The black dashed line indicates the point where wound area and mean fluorescence change at the same rate. Error bars, SEM. (H, I) Total myosin (H) and F-actin (I) fluorescence in the purse string in late embryos decreased only slightly during wound closure. Note the different scales in the *x*- and *y*-axes with respect to D and E. (J, K) Mean myosin (J) and F-actin (K) fluorescence in the purse string in late embryos increased during wound closure. Insets, ratio of the rates of change of wound perimeter to the rate of change of mean myosin (J) or F-actin (K) fluorescence. The black dashed line indicates the point where wound perimeter and mean fluorescence change at the same rate. Error bars, SEM. (A, B, D–K) Embryos expressed both GFP:moesin and myosin:mCherry. Different colors indicate different wounds. Circles indicate the onset of wound closure. (D–K) Data were smoothed using a Gaussian filter with $\sigma = 15$ s. Here $t = 0$ min indicates the onset of wound closure. (L) Fold change in total myosin (red) and F-actin (blue) levels in medial networks in early embryos or purse strings in late embryos during wound repair. Error bars, SEM. (M, N) myosin:mCherry in a medial network in an early embryo (M) and a purse string in a late embryo (N). Times shown in minutes after wounding. Anterior, left; ventral, down. Bar, 2 μm.

in which the forces that drive wound closure are primarily generated by a contractile actomyosin purse string in the absence of a contribution from the wounded cells. These results suggest that the simultaneous and rapid contraction of an actomyosin purse string and medial actomyosin networks in the wounded cells may account for the faster rates of wound closure in early embryos.

These studies define the force-generating cellular structures that contribute to the closure of multicellular wounds and provide the first demonstration that wounded cells actively participate in wound repair. These results are reminiscent of mechanisms of epithelial closure during development, such as the apical constriction of amnioserosa cells at the dorsal surface of the *Drosophila* embryo, which promotes dorsal closure (Toyama *et al.*, 2008; Solon *et al.*, 2009; Blanchard *et al.*, 2010; David *et al.*, 2010). In addition, although actomyosin purse strings are present during wound healing in many systems (Martin and Lewis, 1992; Bement *et al.*, 1993; Brock *et al.*,

1996; Danjo and Gipson, 1998; Kiehart *et al.*, 2000; Russo *et al.*, 2005), they were shown to generate force only during the repair of subcellular wounds in *Xenopus* oocytes (Mandato and Bement, 2001), and the mechanisms that drive force generation during multicellular wound healing were largely unknown. Our findings reveal that both purse-string contractility and medial actomyosin networks in wounded cells generate mechanical forces that promote wound closure and show that the apical constriction of wounded cells accelerates tissue repair in the early *Drosophila* embryo.

Actomyosin contractility is essential for wound repair in early embryos. This is in contrast with late embryos, in which inhibiting myosin activity slows wound repair but does not prevent it (Wood *et al.*, 2002; Abreu-Blanco *et al.*, 2012). In the absence of myosin contractility in the late embryo, wound repair is driven by the zipping of actin-based protrusions that interdigitate at the corners of the wound (Wood *et al.*, 2002; Abreu-Blanco *et al.*, 2012). By contrast, protrusive activity is not sufficient to drive wound repair in the absence of actomyosin contractility in early embryos. The distinct requirements for actomyosin contractility at different stages could be due to differences in the organization and function of the actomyosin machinery, differences in the compensatory mechanisms that contribute to wound closure in the absence of actomyosin contractility, or differences in the extent of actomyosin inhibition in different studies. Of note, wound repair in single-cell *Drosophila* embryos also requires actomyosin contractility (Abreu-Blanco *et al.*, 2011), suggesting that the requirement for contractile networks is a general feature of wound repair early in development.

Our results indicate that the mechanisms of actomyosin contraction change as embryos develop, with network disassembly playing a dominant role in the early embryo and network condensation driving contraction in the late embryo. These results may reflect changes in the molecular machinery that promotes actomyosin contraction. For instance, the actin depolymerizing and severing factor cofilin (Elam *et al.*, 2013) could be more important for wound repair in early embryos, whereas actin cross-linkers such as α-actinin or fimbrin, which stabilize actin filaments (Biron and Moses, 2004; Laporte *et al.*, 2012), may be more important for wound repair in the late embryo. It will be informative to determine the role of actin and myosin regulators in wound repair at different stages of development.

The shape, behavior, and junctional composition of epithelial cells change during development, and these changes may influence the wound repair response. In early embryos, epidermal cells undergo intercalary cell rearrangements that promote axis elongation (Irvine and Wieschaus, 1994), whereas in late embryos cells are relatively static (Simone and DiNardo, 2010; Marcinkevicius and Zallen, 2013). Adherens junctions are more dynamic in early embryos (Huang *et al.*, 2011), which could accelerate junctional disassembly and wound closure. Adherens junctions in early embryos form "spot" complexes (Tepass and Hartenstein, 1994) that could serve as functional anchor points for medial contractile networks (Martin *et al.*, 2010). Spot junctions are rarely observed in the epidermis of late embryos, and this may cause a less efficient engagement of medial networks and adherens junctions at this stage. In addition, cells in the late embryo have septate junctions (Tepass and Hartenstein, 1994), which are associated with proteins such as Discs large and Lethal giant larvae that may negatively regulate myosin activity (Ohshiro *et al.*, 2000; Peng *et al.*, 2000; Simone and DiNardo, 2010). Furthermore, cells in the late embryo contain extracellular matrix proteins that could slow down wound repair (Leptin *et al.*, 1989; Fox *et al.*, 1999). Comparing the role of adhesion molecules in the assembly and contraction of actomyosin networks during wound repair in early and late embryos will determine whether cell–cell and cell–matrix adhesion influence the mechanisms of wound closure.

A striking feature of epidermal wound healing is that its efficiency decays with age. In humans, epidermal wounds in embryos are rapidly repaired with no inflammatory response or scar formation (Rowlatt, 1979). By contrast, wound closure in adults is a slow process that involves inflammation and scarring. We demonstrate that rapid contraction and disassembly of medial myosin networks are associated with faster rates of wound healing than purse-string condensation, and both medial networks and purse strings contribute to rapid wound repair in the early *Drosophila* embryo. Elucidating the molecular and cellular mechanisms of embryonic wound repair may have implications for the development of therapies to accelerate wound healing in adults through the manipulation of signaling pathways that govern actomyosin localization and dynamics.

MATERIALS AND METHODS

Fly stocks

We used the following markers for live imaging: *ubi-E-cadherin:GFP* (Oda and Tsukita, 2001), *sqh-sqh:mCherry* (Martin *et al.*, 2009), *sqh-GFP:Moesin* (*spaghetti squash* driven, GFP, moesin-α-helical-coiled, and actin-binding site, or sGMCA; Kiehart *et al.*, 2000), and *sqh-sqh:GFP* (Royou *et al.*, 2004). Embryos expressing *UASp-GFP:Rho1* (#9392; Bloomington *Drosophila* Stock Center, Bloomington, IN) were the F2 progeny of *UASp-GFP:Rho1* males by *matα.tub67;15* females (gift of D. St Johnston, University of Cambridge).

Time-lapse imaging

Embryos were dechorionated in 50% bleach for 2 min and transferred to a drop of 1:1 halocarbon oil 27:700 (Sigma-Aldrich, St. Louis, MO) on a coverglass. Embryos were oriented with their ventral-lateral side down and mounted on an oxygen-permeable membrane (YSI, Yellow Springs, OH). Similar results were obtained when embryos were glued to a coverglass using heptane glue and imaged without additional flattening. GFP was excited with an argon line (488 nm, 100 mW; Melles Griot, Albuquerque, NM). mCherry was excited with a krypton laser (568 nm, 1 mW; Melles Griot). A 63× oil immersion lens (numerical aperture [NA] 1.4; Carl Zeiss, Jena, Germany) mounted on an UltraView RS5 spinning disk system (PerkinElmer, Waltham, MA) equipped with an Orca ER camera (Hamamatsu, Hamamatsu, Japan) was used for imaging. Sixteen-bit, two-color *Z*-stacks were acquired at 0.5-µm steps every 15 s and projected for analysis (13 slices/stack).

Embryo injections

Embryos were dechorionated in 50% bleach for 2 min and aligned on an apple juice–agar pad, transferred to a coverslip coated with heptane glue, and dehydrated for 10–12 min. Embryos were covered in 1:1 halocarbon oil 27:700 (Sigma-Aldrich) and imaged in a Revolution XD spinning disk confocal (Andor, Belfast, United Kingdom) equipped with an iXon Ultra 897 camera (Andor), a Transferman NK2 micromanipulator (Eppendorf, Hauppauge, NY), and a PV820 microinjector (WPI, Sarasota, FL). A 60× oil immersion lens (NA 1.35; Olympus, Tokyo, Japan) was used for imaging. Sixteen-bit, two-color *Z*-stacks were acquired at 0.3-µm steps every 15 s and projected for analysis (15 slices/stack). Embryos were injected in the perivitelline space with 100–200 pl of 100 mM Y-27632 (Tocris, Ellisville, MO) in water. Control embryos were injected with water. Drugs are predicted to be diluted 50-fold in the embryo (Foe and Alberts, 1983).

Wound delineation and quantification

All the algorithms were developed using Matlab (MathWorks, Natick, MA) and DIPImage (Delft University of Technology, Delft, Netherlands) and were integrated in our custom Scientific Image Segmentation and Analysis (SIESTA) software (Fernandez-Gonzalez and Zallen, 2011). We used the LiveWire algorithm implemented in SIESTA (Fernandez-Gonzalez and Zallen, 2011) for semiautomated tracing of wounds. Briefly, the user moves the mouse pointer around the wound, and the algorithm automatically identifies, in real time, the brightest pixels that follow the trajectory of the mouse (Supplemental Movie S6). The user can approve sections of the contour by clicking with the mouse, which accelerates computational processing by restricting the area of the image under consideration to that bounded by the coordinates of the previous and current positions of the mouse.

Cell areas were quantified using the watershed algorithm in SIESTA (Fernandez-Gonzalez and Zallen, 2011). To quantify protein levels, we divided wounds into two compartments. The purse-string compartment was determined by a three-pixel-wide (0.6 μm) dilation of the wound outline. The medial compartment was obtained by inverting a binary image representing the purse-string compartment and filling the hole in the resulting image using binary propagation. Mean fluorescence was the mean pixel value in each compartment background-subtracted using the image mode as the background and corrected for photobleaching by dividing by the mean pixel value of the entire image. Intensities were normalized to the mean value of each structure in the time-lapse sequence to compare wounds from different embryos. Total fluorescence was the product of mean fluorescence and area or perimeter of the compartment under consideration. Changes in total F-actin and myosin fluorescence were outside the photobleaching range calculated as the change in mean image intensity during image acquisition (1.10 ± 0.02 for F-actin and 1.02 ± 0.01 for myosin).

To distinguish between the fast and slow phases of wound closure, we manually identified the time in which wound closure began. A line was automatically fit to the wound area curve starting from the initial wound closure time. The end of the fast phase was determined as the time in which the correlation coefficient between the wound area curve and the fit line was <0.98. To quantify the rate of wound area contraction in Figure 2D, we took the ratio area(t – 1 min)/area(t) and averaged all the values for each wound at all time points from 3 min after ablation until the end of wound closure at 15-s intervals. Perimeter change was similarly measured. To quantify the increase in mean myosin fluorescence, we used the ratio myosin(t)/myosin(t – 1 min) to account for the fact that area and mean fluorescence are inversely correlated.

Laser ablation

An N_2 MicroPoint laser (Photonic Instruments, St. Charles, IL) tuned to 365 nm was used to wound cells and cytoskeletal networks as described (Fernandez-Gonzalez *et al.*, 2009). The laser delivers 120-μJ pulses with a duration of 2–6 ns each, producing wounds of ~1 μm in diameter. To wound cells, 10 laser pulses were delivered at three or four spots 2 μm apart along a line that crosses a cell interface parallel to the dorsal–ventral axis of the embryo. This generated a 7- to 8-μm linear damage region. To measure the contractile force generated by medial networks and purse strings, we ablated a single spot in the structure in question. Low-power ablations (Supplemental Movies S4 and S5) were done by a single laser pulse at three spots. These were the minimum conditions that caused ablation of cell interfaces as determined by a visible retraction of the severed ends of the interface and the connected vertices.

The initial velocity of displacement after laser ablation can be used to quantify the amount of tension released (Hutson *et al.*, 2003; Fernandez-Gonzalez *et al.*, 2009). We implemented a custom particle image velocimetry algorithm in SIESTA to quantify the velocity of myosin particles around the wound within the first 4 s after ablation (670-ms laser ablation + 3.3-s image acquisition). Pixels 3–5 μm from the ablation site were considered for velocimetry analysis to account for the material destroyed by ablation and the local effect of force relaxation. The velocity field calculated had a spatial resolution of 0.2 μm × 0.2 μm, and >1250 velocity vectors were measured per experiment. For each experiment, the average magnitude of the radial component of the velocity vectors was considered the initial velocity of displacement induced by ablation.

Statistical analysis

To compare time curves, we used the area under each curve as the test statistic. Sample variances were compared using the F test (Glantz, 2002). Sample means were contrasted using Student's t test, applying Holm's correction when three or more groups were considered. The relative correlations and rates of change of wound area or perimeter and medial or purse-string myosin fluorescence were compared using a paired t test. The fold changes of actin and myosin during network contraction were compared between early and late embryos using the Mann–Whitney rank-sum test. We compared the wound size distribution in early and late embryos using the Kolmogorov–Smirnov test. Error bars indicate SEM.

ACKNOWLEDGMENTS

We are grateful to Danielle Hayes for help with the quantification of cell areas. We thank K. Goodwin, T. Harris, H.-P. Hu, M. Hunter, K. Kasza, E. Marcinkevicius, S. Simoes, M. Tamada, U. Tepass, and T. Zulueta-Coarasa for comments on the manuscript. FlyBase provided important references. This work was supported by a W. M. Keck Foundation Distinguished Young Scholar in Medical Research Award to J.A.Z., startup funds from the University of Toronto and the Hospital for Sick Children to R.F.G., and grants from the Canada Foundation for Innovation and the Ontario Research Fund to R.F.G. J.A.Z. is an Early Career Scientist of the Howard Hughes Medical Institute.

REFERENCES

Abreu-Blanco MT, Verboon JM, Liu R, Watts JJ, Parkhurst SM (2012). *Drosophila* embryos close epithelial wounds using a combination of cellular protrusions and an actomyosin purse string. J Cell Sci 125, 5984–5997.

Abreu-Blanco MT, Verboon JM, Parkhurst SM (2011). Cell wound repair in *Drosophila* occurs through three distinct phases of membrane and cytoskeletal remodeling. J Cell Biol 193, 455–464.

Amano M, Ito M, Kimura K, Fukata Y, Chihara K, Nakano T, Matsuura Y, Kaibuchi K (1996). Phosphorylation and activation of myosin by Rho-associated kinase (Rho-kinase). J Biol Chem 271, 20246–20249.

Bement WM, Forscher P, Mooseker MS (1993). A novel cytoskeletal structure involved in purse string wound closure and cell polarity maintenance. J Cell Biol 121, 565–578.

Bement WM, Mandato CA, Kirsch MN (1999). Wound-induced assembly and closure of an actomyosin purse string in *Xenopus* oocytes. Curr Biol 9, 579–587.

Biron D, Moses E (2004). The effect of alpha-actinin on the length distribution of F-actin. Biophys J 86, 3284–3290.

Blanchard GB, Murugesu S, Adams RJ, Martinez-Arias A, Gorfinkiel N (2010). Cytoskeletal dynamics and supracellular organisation of cell shape fluctuations during dorsal closure. Development 137, 2743–2752.

Brock J, Midwinter K, Lewis J, Martin P (1996). Healing of incisional wounds in the embryonic chick wing bud: characterization of the actin purse-string and demonstration of a requirement for Rho activation. J Cell Biol 135, 1097–1107.

Burkel BM, Benink HA, Vaughan EM, von Dassow G, Bement WM (2012). A Rho GTPase signal treadmill backs a contractile array. Dev Cell 23, 384–396.
Burnside B (1971). Microtubules and microfilaments in newt neuralation. Dev Biol 26, 416–441.
Calvert ME, Wright GD, Leong FY, Chiam KH, Chen Y, Jedd G, Balasubramanian MK (2011). Myosin concentration underlies cell size-dependent scalability of actomyosin ring constriction. J Cell Biol 195, 799–813.
Carvalho A, Desai A, Oegema K (2009). Structural memory in the contractile ring makes the duration of cytokinesis independent of cell size. Cell 137, 926–937.
Danjo Y, Gipson IK (1998). Actin "purse string" filaments are anchored by E-cadherin-mediated adherens junctions at the leading edge of the epithelial wound, providing coordinated cell movement. J Cell Sci 111 (Pt 22), 3323–3332.
David DJ, Tishkina A, Harris TJ (2010). The PAR complex regulates pulsed actomyosin contractions during amnioserosa apical constriction in *Drosophila*. Development 137, 1645–1655.
Davidson LA, Ezin AM, Keller R (2002). Embryonic wound healing by apical contraction and ingression in *Xenopus laevis*. Cell Motil Cytoskeleton 53, 163–176.
Elam WA, Kang H, De la Cruz EM (2013). Biophysics of actin filament severing by cofilin. FEBS Lett 587, 1215–1219.
Fernandez-Gonzalez R, Simoes Sde M, Roper JC, Eaton S, Zallen JA (2009). Myosin II dynamics are regulated by tension in intercalating cells. Dev Cell 17, 736–743.
Fernandez-Gonzalez R, Zallen JA (2011). Oscillatory behaviors and hierarchical assembly of contractile structures in intercalating cells. Phys Biol 8, 045005.
Foe VE, Alberts BM (1983). Studies of nuclear and cytoplasmic behaviour during the five mitotic cycles that precede gastrulation in *Drosophila* embryogenesis. J Cell Sci 61, 31–70.
Fox GL, Rebay I, Hynes RO (1999). Expression of DFak56, a *Drosophila* homolog of vertebrate focal adhesion kinase, supports a role in cell migration in vivo. Proc Natl Acad Sci USA 96, 14978–14983.
Glantz SA (2002). Primer of Biostatistics, New York: McGraw-Hill.
Hildebrand JD (2005). Shroom regulates epithelial cell shape via the apical positioning of an actomyosin network. J Cell Sci 118, 5191–5203.
Huang J, Huang L, Chen YJ, Austin E, Devor CE, Roegiers F, Hong Y (2011). Differential regulation of adherens junction dynamics during apical-basal polarization. J Cell Sci 124, 4001–4013.
Hutson MS, Tokutake Y, Chang MS, Bloor JW, Venakides S, Kiehart DP, Edwards GS (2003). Forces for morphogenesis investigated with laser microsurgery and quantitative modeling. Science 300, 145–149.
Irvine KD, Wieschaus E (1994). Cell intercalation during *Drosophila* germband extension and its regulation by pair-rule segmentation genes. Development 120, 827–841.
Kiehart DP, Galbraith CG, Edwards KA, Rickoll WL, Montague RA (2000). Multiple forces contribute to cell sheet morphogenesis for dorsal closure in *Drosophila*. J Cell Biol 149, 471–490.
Kimura K *et al*. (1996). Regulation of myosin phosphatase by Rho and Rho-associated kinase (Rho-kinase). Science 273, 245–248.
Laporte D, Ojkic N, Vavylonis D, Wu JQ (2012). alpha-Actinin and fimbrin cooperate with myosin II to organize actomyosin bundles during contractile-ring assembly. Mol Biol Cell 23, 3094–3110.
Leptin M, Bogaert T, Lehmann R, Wilcox M (1989). The function of PS integrins during *Drosophila* embryogenesis. Cell 56, 401–408.
Longaker MT, Whitby DJ, Adzick NS, Crombleholme TM, Langer JC, Duncan BW, Bradley SM, Stern R, Ferguson MW, Harrison MR (1990). Studies in fetal wound healing, VSecond I, early third trimester fetal wounds demonstrate rapid collagen deposition without scar formation. J Pediatr Surg 25, 63–68; discussion, 68–69.
Ma X, Kovacs M, Conti MA, Wang A, Zhang Y, Sellers JR, Adelstein RS (2012). Nonmuscle myosin II exerts tension but does not translocate actin in vertebrate cytokinesis. Proc Natl Acad Sci USA 109, 4509–4514.
Mandato CA, Bement WM (2001). Contraction and polymerization cooperate to assemble and close actomyosin rings around *Xenopus* oocyte wounds. J Cell Biol 154, 785–797.
Marcinkevicius E, Zallen JA (2013). Regulation of cytoskeletal organization and junctional remodeling by the atypical cadherin Fat. Development 140, 433–443.
Martin AC, Gelbart M, Fernandez-Gonzalez R, Kaschube M, Wieschaus EF (2010). Integration of contractile forces during tissue invagination. J Cell Biol 188, 735–749.
Martin AC, Kaschube M, Wieschaus EF (2009). Pulsed contractions of an actin-myosin network drive apical constriction. Nature 457, 495–499.
Martin P, Lewis J (1992). Actin cables and epidermal movement in embryonic wound healing. Nature 360, 179–183.
Mason FM, Tworoger M, Martin AC (2013). Apical domain polarization localizes actin-myosin activity to drive ratchet-like apical constriction. Nat Cell Biol 15, 926–936.
McCluskey J, Martin P (1995). Analysis of the tissue movements of embryonic wound healing—DiI studies in the limb bud stage mouse embryo. Dev Biol 170, 102–114.
Moreira S, Stramer B, Evans I, Wood W, Martin P (2010). Prioritization of competing damage and developmental signals by migrating macrophages in the *Drosophila* embryo. Curr Biol 20, 464–470.
Oda H, Tsukita S (2001). Real-time imaging of cell-cell adherens junctions reveals that *Drosophila* mesoderm invagination begins with two phases of apical constriction of cells. J Cell Sci 114, 493–501.
Ohshiro T, Yagami T, Zhang C, Matsuzaki F (2000). Role of cortical tumour-suppressor proteins in asymmetric division of *Drosophila* neuroblast. Nature 408, 593–596.
Peng CY, Manning L, Albertson R, Doe CQ (2000). The tumour-suppressor genes lgl and dlg regulate basal protein targeting in *Drosophila* neuroblasts. Nature 408, 596–600.
Pickering K, Alves-Silva J, Goberdhan D, Millard TH (2013). Par3/Bazooka and phosphoinositides regulate actin protrusion formation during *Drosophila* dorsal closure and wound healing. Development 140, 800–809.
Raffel M, Willert CE, Wereley ST, Kompenhans J (2007). Particle Image Velocimetry: A Practical Guide, New York: Springer.
Reichl EM, Ren Y, Morphew MK, Delannoy M, Effler JC, Girard KD, Divi S, Iglesias PA, Kuo SC, Robinson DN (2008). Interactions between myosin and actin crosslinkers control cytokinesis contractility dynamics and mechanics. Curr Biol 18, 471–480.
Robinson DN, Cavet G, Warrick HM, Spudich JA (2002). Quantitation of the distribution and flux of myosin-II during cytokinesis. BMC Cell Biol 3, 4.
Rowlatt U (1979). Intrauterine wound healing in a 20 week human fetus. Virchows Arch A Pathol Anat Histol 381, 353–361.
Royou A, Field C, Sisson JC, Sullivan W, Karess R (2004). Reassessing the role and dynamics of nonmuscle myosin II during furrow formation in early *Drosophila* embryos. Mol Biol Cell 15, 838–850.
Russo JM, Florian P, Shen L, Graham WV, Tretiakova MS, Gitter AH, Mrsny RJ, Turner JR (2005). Distinct temporal-spatial roles for rho kinase and myosin light chain kinase in epithelial purse-string wound closure. Gastroenterology 128, 987–1001.
Simone RP, DiNardo S (2010). Actomyosin contractility and Discs large contribute to junctional conversion in guiding cell alignment within the *Drosophila* embryonic epithelium. Development 137, 1385–1394.
Slattum G, McGee KM, Rosenblatt J (2009). P115 RhoGEF and microtubules decide the direction apoptotic cells extrude from an epithelium. J Cell Biol 186, 693–702.
Solon J, Kaya-Copur A, Colombelli J, Brunner D (2009). Pulsed forces timed by a ratchet-like mechanism drive directed tissue movement during dorsal closure. Cell 137, 1331–1342.
Stramer B, Wood W, Galko MJ, Redd MJ, Jacinto A, Parkhurst SM, Martin P (2005). Live imaging of wound inflammation in *Drosophila* embryos reveals key roles for small GTPases during in vivo cell migration. J Cell Biol 168, 567–573.
Tepass U, Hartenstein V (1994). The development of cellular junctions in the *Drosophila* embryo. Dev Biol 161, 563–596.
Toyama Y, Peralta XG, Wells AR, Kiehart DP, Edwards GS (2008). Apoptotic force and tissue dynamics during *Drosophila* embryogenesis. Science 321, 1683–1686.
Whitby DJ, Ferguson MW (1991). Immunohistochemical localization of growth factors in fetal wound healing. Dev Biol 147, 207–215.
Wood W, Faria C, Jacinto A (2006). Distinct mechanisms regulate hemocyte chemotaxis during development and wound healing in *Drosophila melanogaster*. J Cell Biol 173, 405–416.
Wood W, Jacinto A, Grose R, Woolner S, Gale J, Wilson C, Martin P (2002). Wound healing recapitulates morphogenesis in *Drosophila* embryos. Nat Cell Biol 4, 907–912.
Wu JQ, Kuhn JR, Kovar DR, Pollard TD (2003). Spatial and temporal pathway for assembly and constriction of the contractile ring in fission yeast cytokinesis. Dev Cell 5, 723–734.